Sterically hindered fragmentation in reactive solids

1991 J. Phys. A: Math. Gen. 24 3077

(http://iopscience.iop.org/0305-4470/24/13/022)

J. Phys. A: Math. Gen. 24 (1991) 3077–3093. Printed in the UK

Sterically hindered fragmentation in reactive solids

C A Miller†, A R Kerstein‡ and S Torquato§‖

† Department of Mechanical and Aerospace Engineering, North Carolina State University, Raleigh, NC 27607-7910, USA
‡ Sandia National Laboratories, Livermore, CA 94550, USA
§ Courant Institute of Mathematical Sciences, New York University, New York, NY 10012, USA

Received 9 January 1991

Abstract. A two-dimensional model of a two-phase solid which undergoes a reaction at its surface is used to study the fragmentation of reactive materials in which the morphological hindering of fragment release is considered. Scaling concepts of cluster percolation theory are used to evaluate Monte Carlo data generated from a simulation of the hindered fragmentation process. By defining a hierarchy of fragmentation objects, different scaling exponents are computed for each of these objects as measured by the number of sub-objects they contain. In addition, it appears that each of the different measures of object size exhibits optimum scaling at a different critical reactive-phase mass fraction; simulation data indicate that the critical mass fractions follow a trend consistent with expected physical behaviour of the system. In addition, the critical mass fractions reported correspond to 'virtual' criticalities, i.e. the critical points cannot result in actual divergences in size, but rather are properties of the scaling function.

1. Introduction

The phenomenon of particle fragmentation and its effects on the degradation of porous carbon solids has been given considerable attention in recent years (Chirone *et al* 1982, Kerstein and Niksa 1985, Sundback *et al* 1985, Kerstein and Edwards 1987). The overall rate of pyrolysis, combustion or gasification of such substances can be significantly affected by the sudden release of discrete solid particles from the original 'parent' particle, i.e. the fragmentation of the solid. The ability to describe and predict the fragmentation behaviour of a material is therefore of considerable importance in evaluation of the total degradation process. The mechanisms of fragment formation are dependent upon factors internal to the solid, such as morphology and composition of constituent phases, as well as external factors such as the mechanical stress and the thermochemical environment to which the solid is exposed. Despite these complications, significant predictions of fragmentation behaviour have been made based on purely geometrical considerations (Kerstein and Niksa 1985). However, basic aspects of fragmentation in porous reactive solids have not yet been addressed, one of which is the effect of morphological or steric hindering.

Previous models of the fragmentation process (Kerstein and Niksa 1983, Mekjian 1990, DeAngelis and Mekjian 1989) have been limited to the case of simple fragmentation, in which a fragment newly separated from the original particle is immediately

‖ Permanent address: Department of Mechanical and Aerospace Engineering, North Carolina State University, Raleigh, NC, USA.

0305-4470/91/133077+17$03.50

released to the surrounding environment. In general, a fragment may not find a free path to the ambient surroundings immediately upon its creation. The case may be such that the newly formed fragment, although physically disconnected from the parent, is prevented from being released due to the spatial configuration of the parent particle; such a fragment is said to be *sterically hindered.* The shape of the parent may be such that the release of not only one, but several fragments are hindered simultaneously. The subsequent degradation of a single critical bond may result in the release of a 'burst' of several fragments of various sizes to the surroundings, behaviour which has been observed in experimental studies of dissolution of porous solids (Mills and Kerstein 1990). Models of fragmentation in which hindering is neglected will in general not produce bursts of more than two fragments; consideration of hindering can therefore result in behaviour which is significantly different from that observed in simple-fragmentation models.

At the most basic level, the process of fragmentation is the transition of a solid from a connected state (i.e. a single particle) to a disconnected state in which several particles have evolved from the original parent particle. The principles and methods of percolation theory have been developed specifically to quantify the state of connectedness of irregular objects and systems (Stauffer 1979, 1985, Deutscher *et al* 1983, Essam 1980); it is natural then to employ these principles in evaluating the fragmentation process.

The current study applies the principles of percolation theory to evaluate hindered fragmentation, using Monte Carlo methods to simulate the behaviour of a heterogeneous solid material which undergoes a reaction at its surface. The heterogeneity of the material is due to non-reactive inclusions randomly distributed throughout a continuous reactive matrix; the reaction occurs only on the surface of the reactive material. As the reaction proceeds, the surface morphology becomes increasingly complex, resulting in the creation of fragments and the eventual release of those fragments in bursts. Our objective is to qualitatively describe the relationship between the volume (or mass) fraction ϕ_1 of the reactive phase and the distributions of both the numbers and mass of released fragments, considering the morphological hindering and release of separated fragments. The results show that the objects generated during the fragmentation process do indeed obey the scaling 'laws' of percolation theory (Stauffer 1985). Approximate values of the parameters resulting in the best scaling behaviour are obtained. However, accurate determination of the scaling exponents is outside the scope of the present paper.

The formation of isolated fragments due to the propagation of a reaction interface into a medium is reminiscent of invasion percolation (Nickel and Wilkinson 1983, Wilkinson and Willemsen 1983, Willemsen 1984). As in the present problem, the process of disconnection in invasion percolation is a local phenomenon that is only indirectly related to the global state of connectedness of the phase of the infinite medium through which the interface propagates. In both invasion percolation and the present problem, the aspect of greatest interest is the statistical characterization of the objects that are disconnected from the parent medium as a result of interface motion. Furthermore, confinement of system evolution to a propagating interface renders both problems inherently dynamic.

The fragmentation problem introduces other aspects not found in typical applications of percolation theory. Probability distributions characterizing 'burst' events can be parametrized in terms of a hierarchy of objects and sub-objects (which will be defined below). Here we mention only the two most obvious units of measurement:

(*a*) the total mass release per burst and (*b*) the number of fragments per burst; note that we can further examine the mass distribution of individual fragments within the bursts. A further difference is that, in the fragmentation problem, fragments may be heterogeneous in composition as opposed to the homogeneous clusters ordinarily evaluated in percolation problems; given a heterogeneous parent material composed of reactive and non-reactive elements (phases), fragments of this parent may contain either or both of the phases following separation.

The origin of the hierarchy of objects can be illustrated by comparing the phenomenon of hindering to directed percolation (Kinzel 1983, Williams and Mackenzie 1984). In particular, consider a two-dimensional lattice percolation problem in which the medium has been fragmented by randomly removing a fraction $\phi > \phi^c$ of sites, where ϕ^c is the ordinary (non-directed) static percolation threshold. Designate any given pair of fragments as non-hindering only if some directed path (i.e. a path not allowed to reverse itself in a specified coordinate direction) through the vacant sites separates the fragments; otherwise the fragments are mutually hindering. (This criterion is not quite the same as the hindrance criterion in our fragmentation model.) Assume that $\phi > \phi^d$, where $\phi^d > \phi^c$ is the percolation threshold for directed paths. It is evident that one thus obtains a three-level hierarchy of objects: lattice sites, fragments and mutually hindering groups of fragments. The geometrical properties of hierarchies arising in static problems of this type are themselves of interest, but have not been studied to our knowledge. The hindered percolation process considered here has both a hierarchical nature, reflecting a direction-dependent hindrance criterion, and a dynamical nature, reflecting the limitation of site removal to the evolving surface. The objective is to capture both aspects in a formulation that is a simple paradigm of the physical process of fragmentation in reacting solids.

In the following section, the model system and simulation procedure are described, as well as the hierarchy of fragmentation objects. In section 3, we discuss some basic percolation concepts and their application to the fragmentation problem. Section 4 presents results of the simulation and the scaling behaviour of the system. Finally, in section 5, we make concluding remarks.

2. Simulation model and procedure

A simple two-dimensional lattice model of a heterogeneous solid is employed to study the effects of hindering. A square lattice of side length L is tessellated into square cells of unit area, of which a given area fraction ϕ_2 are randomly selected to be non-reactive cells, the remaining fraction $\phi_1 = 1 - \phi_2$ designated as reactive. In order to simulate a semi-infinite solid, the initial $L \times L$ configuration is periodically repeated in both x directions; extension of the model in the positive-y direction will be discussed below. The lower edge of the lattice is designated to be $y = 0$, and represents the initial solid surface. Two cells are defined to be connected if they share at least one common side and are not connected across corners. Cells correspond to units of mass; in the current study the area fractions ϕ_1 and ϕ_2 are equivalent to their respective mass fractions.

Beginning from this initial configuration, simulation of the surface reaction proceeds as follows. A cell on the initial surface $y = 0$ is randomly chosen, and if reactive is removed from the system, resulting in a new surface configuration. Reactive cells bordering the new surface are now eligible for removal. As this 'reaction' process is repeated, the complexity of the surface shape increases, leading to the generation of

fragments. A fragment is defined as a set of one or more connected cells which are disconnected from the original parent solid. A fragment is considered to be unhindered and free to be released if each cell within the fragment has a free path away from the original lattice in the negative-y direction, i.e. below each cell of the fragment there must be no cells belonging to either the main solid or any other hindered fragment. The release criterion is motivated by an experimental configuration (Kerstein and Niksa 1985, Mills and Kerstein 1990) in which fragments evolve from the lower face of a reacting horizontal slab, falling vertically due to gravity unless they are hindered (i.e. their path is blocked) either by a portion of the parent slab or by other hindered fragments. For example, figure 1 shows three fragments disconnected from the main solid, only one of which is free to be released (fragment 1); note that fragment 3 is hindered only by fragment 2, which is in turn hindered by the parent solid. Fragments which have been released are considered to be removed from the problem; further possible degradation and fragmentation of released fragments are outside the scope of the present study.

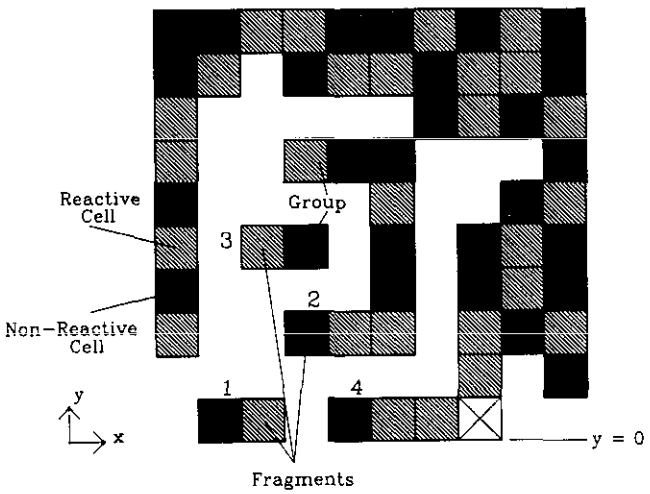

Figure 1. Representation of fragmentation model at an initial reactive mass fraction $\phi_1 = 0.70$. The black and shaded squares represent non-reactive and reactive cells, respectively. The cells labelled '1' compose an unhindered fragment of two cells in size, which is in the process of being released. Fragment '2' is hindered both by fragment '3' and incipient fragment '4'. Fragment 3 is hindered only by fragment 2. If the cell labelled '×' were to be removed, the newly formed fragment 4 would be released, as well as the group composed of fragments 2 and 3. This burst would contain two groups (of one and two fragments, and three and 11 cells, respectively), three fragments, and 14 cells.

As noted above, the hindering of fragments can result in bursts of several fragments being released at a single time. One of the unique aspects of hindered fragmentation is that the size and structure of bursts can be characterized in several different ways, according to a hierarchy of objects and sub-objects. The basic objects of interest are the cells, which may be either reactive or non-reactive. At the next level in the hierarchy is the fragment, which is defined as above to be any connected collection of one or more cells which has become disconnected from the original solid. Fragment size can only be described in terms of the number of cells contained in a fragment; a cell is then referred to as a sub-object of a fragment. A set of one or more fragments may

form a *group*, which is a collection of distinct fragments which are mutually hindering and must therefore be released together. Groups have as sub-objects both fragments and cells, i.e. the size of a group can be characterized by the number of fragments within the group or by the number of cells within the group. At the highest level is a 'burst', which is defined as the totality of fragment objects released from the parent solid at a given instant. A burst can be characterized in terms of each of the lower-level objects: number of groups within a burst, number of fragments within a burst and number of cells within a burst.

An illustration of these objects is presented in figure 1, which shows a representation of the original solid and three separated fragments labelled 1, 2 and 3, containing two, nine and two cells, respectively. Fragments 2 and 3 are hindered from release by the set of cells labelled 4, and by each other; since fragments 2 and 3 cannot separate from each other based on the release criterion, they form a two-fragment group. Since fragment 1 is not hindered, a burst of one fragment consisting of two cells (constituting in this instance a one-fragment group) is in the process of being released. The set of cells labelled 4 composes an incipient fragment, which will be released if the reactive cell marked '×' is decomposed. If this cell were decomposed, the resulting burst could be described in the following ways: two groups, respectively composed of two fragments (2 and 3) and one fragment (4); three fragments (2, 3 and 4) composed of nine, two and three cells, respectively; or fourteen total cells.

After a chosen surface cell is removed, the entire lattice is scanned to determine the effects of that cell's removal. (Removal from hindered fragments as well as from the parent solid is allowed.) The loss of a single reactive cell can result in one of several possibilities: (i) no change in the number or state of hindering of pre-existing fragments, (ii) the formation of one or two new fragments, (iii) the removal of a cell hindering the release of pre-existing fragments, or (iv) a combination of (ii) and (iii) above. Following removal of a reactive cell, the system is scanned to determine the state of connectedness of each cell. In order to save computation time, the connectivity of each new configuration is tested by considering only the cells on the boundary of the solid. Each boundary cell is uniquely labelled, and must be either connected to the parent solid or be part of a separate fragment (which may be a single-cell fragment). A connectivity matrix is formed by checking the connectedness of the boundary cells, and any fragments which have been formed are identified using a connectivity matrix algorithm (Sevick *et al* 1988). Once fragments have been identified, each is checked to determine its state of hindering, and mutually hindering fragments are labelled as groups. Cascade effects must also be considered; for example, if fragment a is hindered only by fragment b, but the removal of a reactive boundary cell has resulted in fragment b becoming unhindered, then a is also unhindered, and both may be released.

If any newly-formed or pre-existing fragments are now free to be released, a burst occurs and the quantities of interest are tabulated. These include the number of fragments in the burst, the total number of cells within those fragments, the size distribution of fragments in terms of cells, and the size distribution of bursts in terms of both cells and fragments as well as analogous quantities for groups. In addition, the time history of each run is recorded by tracking the step number of each burst and the various quantities associated with each particular burst.

Initially, the model is an $L \times L$ square, with the bottom edge of the square at $y = 0$ and periodic boundaries in both x directions. As the surface reaction propagates, the receding surface will eventually reach the $y = L$ layer. At this point, an additional layer of cells is added to the system, with each of the L new cells being randomly designated

as non-reactive with probability ϕ_2. Runs at the lower reactive phase mass fractions often require trials involving several initial configurations, since the configuration of a new layer may be such that a continuous reaction path to larger y values does not exist.

To eliminate the effects of the initial transient period, statistics are not compiled until the time history of the fragmentation process, as reflected by burst statistics, relaxes to a statistically steady state. The overall procedure is then continued until a total of 6250 bursts have occurred, and the results are analysed to estimate the various parameters. The runs were made primarily on an IBM RS6000 workstation, and run times for the total 6250 bursts at a system size $L = 30$ ranged from 2 CPU hours at an reactive-phase area (mass) fraction $\phi_1 = 0.7$ to a maximum of 27 CPU hours at $\phi_1 = 0.6$. Additional runs of 3000 bursts were made on a Cray Y-MP to evaluate the effects of changing the system size, with an average run time on the Cray of 105 CPU minutes for 3000 bursts with a system size of $L = 40$.

3. Application of percolation theory to fragmentation

As noted in the introduction, percolation theory has typically been applied to problems in which the connectivity of static clusters is the primary issue. For static percolation (Stauffer 1985) it is found that, at the percolation threshold ϕ^c (defined as the mass fraction at above which a given phase becomes connected across the lattice), the number density N_S of clusters of size S obeys

$$N_S \propto S^{-\tau} \tag{1}$$

where τ is a universal constant dependent only upon the dimensionality of the system. For the square lattice used here, the site percolation threshold of the ith phase ($i = 1, 2$) has been found to be $\phi^c = 0.593$ (Stauffer 1985). Note that since $\phi^c > 0.5$, there is a range $0.407 < \phi < 0.593$ of phase mass fractions in which neither phase is percolating. Thus, infinite-sized clusters of phase i exist in static (ordinary) percolation problems at or above ϕ^c but not otherwise.

Below the percolation threshold, the number of static percolation clusters of a given size is governed by the scaling relation (Stauffer 1979, 1985)

$$N_S \propto S^{-\tau} f[|\phi_1 - \phi_1^*|^{1/\sigma} S] \tag{2}$$

where the scaling function f is normalized so that $f(0) = 1$, and ϕ_1^* is the critical reactive mass fraction, equivalent to ϕ^c in ordinary static percolation. [Note that at $\phi_1 = \phi_1^*$, relation (2) is identical to relation (1).] As the static percolation threshold is approached, the cluster-size distribution at various values of ϕ_1 near ϕ^c collapse on to a single curve when the data are plotted according to relation (2) (Stauffer 1985); such a collapse of the data is an identifying characteristic of percolation scaling. The exact form of the scaling function f is not known *a priori*, and will be approximated for hindered fragmentation from the simulation data.

In the current problem, we are interested in the behaviour of the system as the reactive mass fraction ϕ_1 nears the critical mass fraction ϕ_1^*, where ϕ_1^* for fragmentation may not be related to ϕ^c in a simple manner. In particular we seek to determine the size distributions of fragmentation objects as a function of ϕ_1 and to assess the applicability of scaling relationships such as (2) above. Unlike static percolation, in which the percolation threshold ϕ^c is the well defined critical point at which the disconnected clusters percolate (i.e. become connected across the lattice), the critical

reactive mass fraction at which the sizes of the fragmentation objects diverge is not as clearly defined.

3.1. Critical reactive mass fraction

Typically, the critical mass (volume or area) fraction of percolation processes is characterized by the divergence of one of the quantities of interest in the particular problem, most frequently the size of a cluster. Considerations other than size can lead to different critical points, however, among these being directional constraints. In directed percolation problems for instance, the path of connectivity which defines the percolating cluster is limited in that only given directions may be chosen (Kinzel 1983, Williams and Mackenzie 1984); a common constraint is that the path may only proceed in the positive x and y directions. A different example is that of invasion percolation, in which the growth of clusters is determined by the path of least resistance as measured by randomly assigning resistances to each lattice site (Nickel and Wilkinson 1983, Wilkinson and Willemsen 1983, Willemsen 1984). In each of these examples, the characteristic criticality is function of not only the lattice geometry, but also the constraints of the particular problem. In the current problem, we are interested in the critical reactive mass fraction at which the various fragmentation objects diverge in size. However, since the size of these objects can be measured in terms of several different sub-objects, the different measures of size may lead to different critical mass fractions.

As noted above, neither the reactive phase nor the non-reactive phase percolates (i.e. is continuous across the sample) in the range $0.407 < \phi_i < 0.593$ $(i = 1, 2)$. For $\phi_1 < \phi^c = 0.593$, the reaction process cannot proceed since the reactive phase is not continuous. At $\phi_1 = \phi^c$, an infinite (system-spanning) cluster of reactive cells exists, allowing propagation of the reaction process.

Although this propagation threshold is directly related to static percolation, criticality associated with the size divergence of fragmentation objects has no obvious relation to a static problem. In the previous section, the symbol ϕ_1^* was introduced to represent a generic critical value of ϕ_1 corresponding to such a divergence. The value of ϕ_1^* will in general depend on the type of fragmentation object being considered and the type of sub-object used to characterize its size.

For instance, consider the divergence of mean fragment size, defined in the usual way. Every connected cluster of non-reactive cells, when eventually released, is entirely contained within a single fragment. A fragment may contain more than one non-reactive cluster, with reactive cells serving to connect those clusters so as to form a single fragment. (It is assured that some reactive cells will survive the removal process and be available to form such connections, because reactive cells that are not part of the percolating reactive network are never removed.) Therefore the fragment size will diverge up to values of ϕ_1 as large or higher than the maximum value $1 - \phi^c$ for size divergence of non-reacting clusters. The maximum value ϕ_1^* for fragment divergence must therefore fall within the range $[1 - \phi^c, \phi^c]$. The upper bound reflects the fact that, for $\phi_1 > \phi^c$, the propagation of the reacting interface along connected paths tessellates the plane into finite regions, thus bounding the size of fragments. (The significance of criticality at a value of ϕ_1 for which the reaction cannot proceed is discussed shortly.)

The lower bound on the critical values ϕ_1^* governing the divergences of mean group size and mean burst size is governed by analogous considerations. For these quantities,

however, ϕ^c is not necessarily an upper bound on the critical reactive mass fraction. Tessellation of the plane by undirected connected paths does not entirely eliminate the directionally-defined hindrances among the finite regions, so criticality for these objects may occur above ϕ^c.

Since bursts are at the highest level of the fragmentation object hierarchy, and have as sub-objects all other fragmentation objects, the size as expressed in terms of cells will clearly diverge at a reactive mass fraction greater than or equal to the mass fractions at which groups and fragments, so expressed, will diverge. Therefore, it is expected that the following relation between the critical mass fractions will hold:

$$\phi_1^*(b, c) \geq \phi_1^*(g, c) \geq \phi_1^*(f, c) \tag{3}$$

where $\phi_1^*(x, y)$ denotes the critical reactive mass fraction of x-type objects when size is measured in terms of y-type sub-objects (b, g, f and c denote burst, group, fragment and cell, respectively). Note that it is possible that some of the critical reactive mass fractions in (3) may lie above the percolation threshold ϕ^c, based on the discussion of the previous paragraph. We also note that the critical reactive mass fraction $\phi_1^*(b, f)$ for bursts with size expressed in terms of fragments should be less than or equal to $\phi_1^*(b, c)$, following the same arguments given above. Therefore it is expected that as one measures bursts in terms of increasingly smaller sub-objects, the following relation will hold:

$$\phi_1^*(b, c) \geq \phi_1^*(b, f) \geq \phi_1^*(b, g). \tag{4}$$

In summary, the critical reactive mass fraction $\phi_1^*(x, y)$ may be different for each pair (x, y) and, if such differences exist, they are expected to obey relations (3) and (4). In addition, if any critical mass fraction $\phi_1^*(x, y)$ appears to be less than ϕ^c, then for that case we have the interesting phenomenon of 'virtual' criticality, i.e. criticality that cannot manifest itself as a literal divergence since the model reaction does not propagate for $\phi_1 \leq \phi^c$, but arises as a property of the scaling function. Thus the critical reactive phase mass fraction is a further variable which must be determined, in addition to the scaling exponents τ and σ arising in (2).

4. Results

As noted above, simulation data were gathered over a total of 6250 bursts for a number of variables. Recorded at each burst were the size of the burst in terms of its respective sub-objects, the size of each group in terms of fragments and cells, and the size of each fragment as measured in cells. These objects and their respective units of measure will be denoted as the size $S(x, y)$ of a type-x object in terms of the number of type-y sub-objects that it contains, and $N_{S(x,y)}$ as the number density of type-x objects of 'y-size' $S(x, y)$. Note that these quantities refer to ensemble averages over all bursts.

Figure 2 presents simulation data for the mean burst and fragment sizes in terms of cells $S(b, c)$ and $S(f, c)$, respectively, and the mean burst size in terms of fragments $S(b, f)$, as a function of the reactive mass fraction ϕ_1. As expected, the values of $S(b, c)$ are significantly higher than $S(f, c)$ at a given mass fraction, with the difference increasing as the reactive mass fraction is decreased. If hindering were not considered, i.e. a fragment was released immediately upon generation, the two lines would be almost identical. In the square lattice model considered here, the removal of a single reactive cell when hindering is neglected could result in the release of no more than

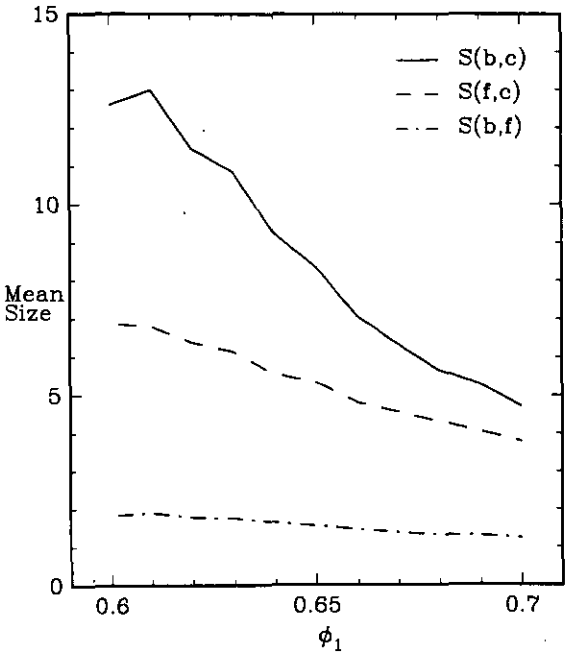

Figure 2. Mean size of fragmentation objects as a function of reactive mass fraction ϕ_1. The mean burst size in terms of cells $S(b, c)$ is given by the solid line (——), the mean fragment size in terms of cells $S(f, c)$ by the dashed line (- - - -), and the mean burst size in terms of fragments $S(b, f)$ by the dot-dashed line (—·—).

two fragments in a single burst, a situation which would be relatively rare. Thus, $S(b, c)$ in the case of no hindering would be closely approximated by $S(f, c)$. Also, in the case of no hindering, $S(b, f)$ would approach a constant value of 1, since in that instance $S(b, c) \simeq S(f, c)$. The effects of hindering in this model are therefore immediately apparent from figure 2. Data for burst size in terms of groups and for groups in terms of fragments is not presented here. The mean size of a group as measured in fragments $S(g, f)$ was found to be almost identically 1 for all values of ϕ_1, and the above mean sizes involving fragments are approximately the same as those involving groups.

4.1. Scaling of fragmentation results

In figures 3–5, size distributions for bursts and fragments in terms of cells, and bursts in terms of fragments are presented, respectively. The ensemble-averaged number density of given size objects $N_{S(x,y)}$ is plotted against the object size $S(x, y)$ on a log–log scale. In each plot, the data are collected into bins which contain a range of object sizes: $S(x, y) = 1$, 2–3, 4–7, 8–15, 16–31, ... Again, data for bursts as expressed in terms of groups, and for groups in terms of fragments and cells are not presented, due to the close similarity of fragments and groups.

Figure 3 plots the number density of fragments of a given size $N_{S(f,c)}$ as a function of the size $S(f, c)$ for reactive phase mass fractions $0.6 \leqslant \phi_1 \leqslant 0.7$. It is clear from this plot that the slopes of the curves are almost identical for the smaller size ranges. For $S(f, c) > 32$, however, the data diverge, with the occurrence of large fragments being more frequent for the lower reactive cell mass fractions.

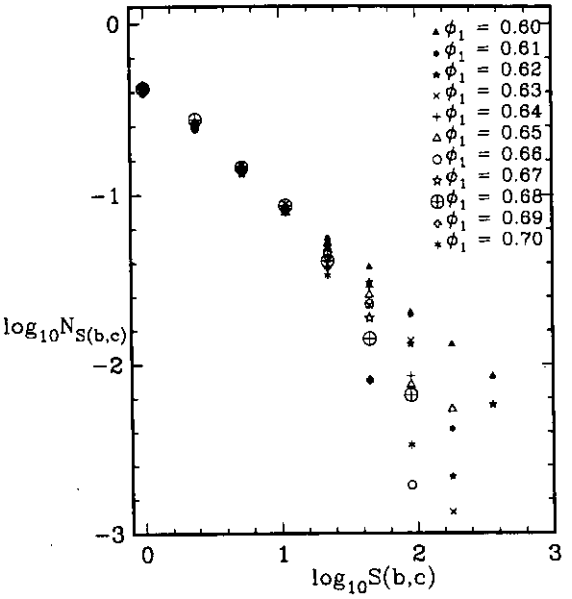

Figure 3. Size distribution of the size of fragments in terms of cells, $S(f, c)$ for different values of reactive mass fraction ϕ_1. For $S(f, c) < 64$, the slope of the line is $\tau = 1.4$.

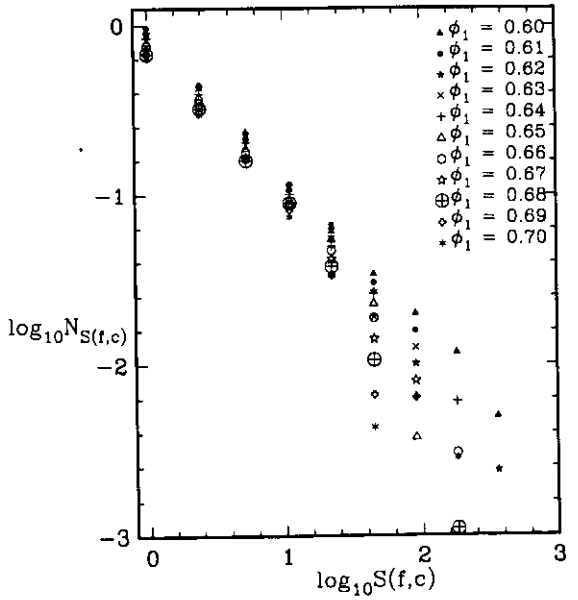

Figure 4. Size distribution of the size of bursts in terms of cells, $S(b, c)$ for different values of reactive mass fraction ϕ_1. For $S(b, c) < 64$, the slope of the line is $\tau = 1.1$.

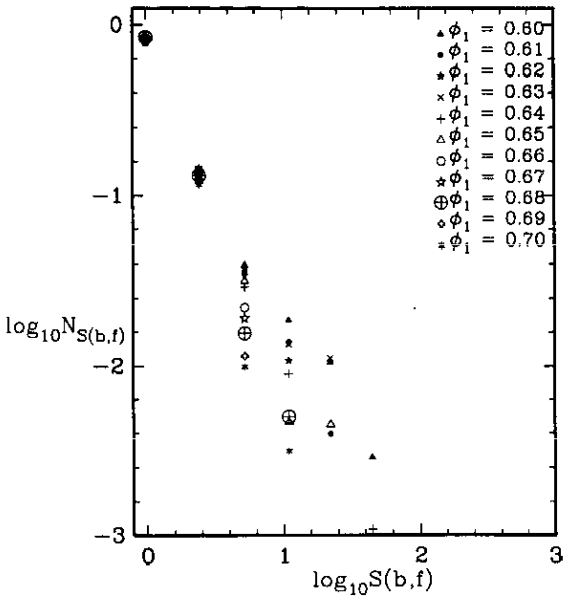

Figure 5. Size distribution of the size of bursts in terms of fragments, $S(b,f)$ for different values of reactive mass fraction ϕ_1. For $S(b,f)<8$, the slope of the line is $\tau=3.1$.

In figure 4, the number density of bursts of a given size in terms of cells $N_{S(b,c)}$ is plotted against the size $S(b, c)$ for the cases of ϕ_1 as above. In this case, the distributions for $S(b, c)<32$ are very close for all values of ϕ_1, and again show the linear behaviour in this range. Again the data diverge above this point, with the lower reactive phase mass fractions generating significantly more large bursts than the higher values of ϕ_1, as expected.

The data presented in figures 3 and 4 illustrate two interesting points. At the lowest reactive mass fraction plotted ($\phi_1=0.60$), the size distributions for both bursts and fragments as expressed in cells, $S(b, c)$ and $S(f, c)$, respectively, are quite linear over the entire range of sizes when the data are plotted on a log–log scale. This is reasonable in light of relations (1) and (2); as the difference $|\phi_1-\phi_1^*|$ decreases, one would expect that the size distribution would approach such a linear behaviour. The second point is that, for the smaller size ranges (i.e. $S<32$), the data at all values of reactive mass fraction tend to follow the same slope as the lowest reactive mass fraction note above. Relation (1), although true only at the percolation threshold, can then provide a relatively accurate relation for the size distribution of the smaller fragmentation objects (i.e. $S(x, c)\leqslant 32$, $x=b, c$) for a wide range of reactive phase mass fraction ϕ_1. Adopting the notation $\tau(x, y)$ to represent the exponent of relation (1) for size distributions of objects x in terms of sub-objects y [i.e. $\tau(b, c)$ would represent the exponent for burst sizes in terms of cells $S(b, c)$], we find the values of $\tau(x, y)$ for the smaller object sizes to be as given in table 1.

Figure 5 presents the number of bursts of a given size in terms of fragments $N_{S(b,f)}$ as a function of size, again for the above mass fractions. As in the two previous distributions, these data are very similar for the lower sizes, although the divergence here occurs at a much lower size. This is reasonable, since fragments are composed of lower-order objects (cells). A burst of 10 fragments will be a much less frequent event than a burst of 10 cells, since a significant amount of hindering must take place

Table 1. Values of the exponent $\tau(x, y)$ for size distributions of various fragmentation objects at the smaller size ranges. Here $\tau(x, y)$ is defined by relation (1), with subscripts denoting the size of the objects x in terms of sub-objects y.

(x, y)	Size range	$\tau(x, y)$
(b, c)	$1 \leqslant S(b, c) \leqslant 32$	1.12
(g, c)	$1 \leqslant S(g, c) \leqslant 32$	1.42
(f, c)	$1 \leqslant S(f, c) \leqslant 32$	1.42
(b, g)	$1 \leqslant S(b, g) \leqslant 8)$	3.09
(b, f)	$1 \leqslant S(b, f) \leqslant 8$	3.05

for such a large burst of fragments to occur. At a reactive mass fraction $\phi_1 = 0.6$, for example, out of a total of 6250 bursts, 12 bursts of 10 fragments in size occurred as compared with 67 bursts of 10 cells in size (i.e. $N_{S(b,f)=10} = 12$ and $N_{S(b,c)=10} = 67$). In the case of bursts in terms of fragments, the sensitivity of the number density to reactive mass fraction begins to appear for bursts of as few as four fragments.

In the previous section, relation (2) was introduced as the scaling relation for reactive mass fractions below the percolation threshold ϕ^c. As has been noted, the system must always be above the reactive phase percolation threshold in order for the reaction process to propagate. However, if one considers the critical mass fraction of (2) to be that at which the quantity of interest (here the size of the fragmentation objects) diverges, then as clearly seen in the plots of mean object size the system is below the critical mass fraction. Thus it is appropriate to utilize relation (2) or a similar relation as the basis for scaling of the fragmentation objects.

If fragmentation is a percolation-type process, it is expected that use of the scaling relation (2) will result in plots in which data for all mass fractions lie on a single curve. Recasting relation (2) in terms of the fragmentation variables defined above yields

$$N_{S(x,y)} \propto S(x, y)^{-\tau(x,y)} f_{(x,y)}[|\phi_1 - \phi_1^*|^{1/\sigma(x,y)} S(x, y)] \tag{5}$$

where $\tau(x, y)$ and $\sigma(x, y)$ denote the scaling exponents for sizes of type-x objects as expressed in type-y sub-objects, and $f_{(x,y)}$ is the scaling function; here f is a function of the objects x and sub-objects y, as opposed to the static percolation case of relation (2). Note also that both $N_{S(x,y)}$ and $S(x, y)$ are functions of mass fraction ϕ_1. Values of τ and σ were determined by plotting $N_S S^\tau$ against $(\phi_1 - \phi_1^*)^{1/\sigma} S$ [it is understood that here N, S, τ and σ are functions of (x, y)], and determining the third-order polynomial which best fit the data points in a least-squares sense. Squares of the errors between the value of each data point and the polynomial were then summed for each candidate set of values of ϕ_1^*, τ and σ. The values of ϕ_1^*, τ and σ which resulted in the minimum squared error are used as the best parameters for the two curves. In table 2, we present a summary of the scaling exponents and critical reactive phase mass fractions which yielded the best agreement with (5) for each of the combinations of fragmentation objects. Note that we do not consider these values to be 'exact'. The relatively small number of bursts generated for this study, while providing good data with which to evaluate the general behaviour of the fragmentation process, are not large enough to yield highly accurate results for the scaling parameters. Nonetheless, the values presented in table 2 do provide valuable information concerning the overall behaviour of fragmentation.

Table 2. Values of the scaling exponents $\tau(x, y)$, $\sigma(x, y)$ and critical reactive mass fractions $\phi_1^*(x, y)$ for different fragmentation objects as expressed in terms of their constituent sub-objects. Here the quantities in parentheses denote the value for objects of type x as expressed in sub-objects of type y. The distribution of groups in terms of fragments did not yield data which was adequate for scaling.

(x, y)	$\tau(x, y)$	$\sigma(x, y)$	$\phi_1^*(x, y)$
(b, c)	0.65	0.36	0.57
(g, c)	0.79	0.36	0.56
(f, c)	0.78	0.28	0.53
(b, g)	1.49	0.11	0.41
(b, f)	1.58	0.21	0.58

Figures 6 and 7 present scaling plots of the fragmentation object size distributions for bursts and fragments, respectively, in terms of cells. By plotting $N_{S(x,y)}S(x, y)^{\tau(x,y)}$ against $(\phi_1 - \phi_1^*)^{1/\sigma(x,y)}S(x, y)$, the values of the scaling exponents $\tau(x, y)$ and $\sigma(x, y)$ which provide the best collapse of the data can be determined. Both data sets show relatively good collapse for all values of reactive phase mass fraction ϕ_1. For the distribution of burst sizes in terms of cells, the values of $\tau(b, c) = 0.64$, $\sigma(b, c) = 0.36$ and $\phi_1^*(b, c) = 0.57$ resulted in the best scaling behaviour. For fragments in terms of cells, the best collapse was obtained when $\tau(f, c) = 0.78$, $\sigma(f, c) = 0.28$ and $\phi_1^*(f, c) = 0.53$. A comparison of figures 6 and 7 shows the similarity in scaling of both bursts and fragments in terms of cells. The best scaling for groups as expressed in cells was found to occur for $\tau(g, c) = 0.79$, $\sigma(g, c) = 0.36$ and $\phi_1^*(g, c) = 0.56$. The scaling plot of groups in terms of cells is not presented due to its close similarity to both bursts

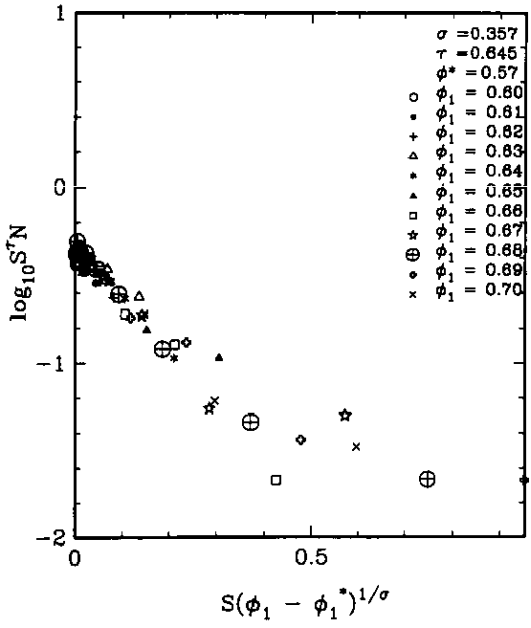

Figure 6. Scaling plot of the burst size in terms of cells $S(b, c)$. Here $\log_{10} S(b, c)^{\tau(b,c)}N_{S(b,c)}$ is plotted as a function of $[\phi_1 - \phi_1^*(b, c)]^{1/\sigma(b,c)}S(b, c)$ as in relation (5). The best collapse of the data is for $\sigma(b, c) = 0.36$, $\tau(b, c) = 0.65$ and $\phi_1^*(b, c) = 0.57$.

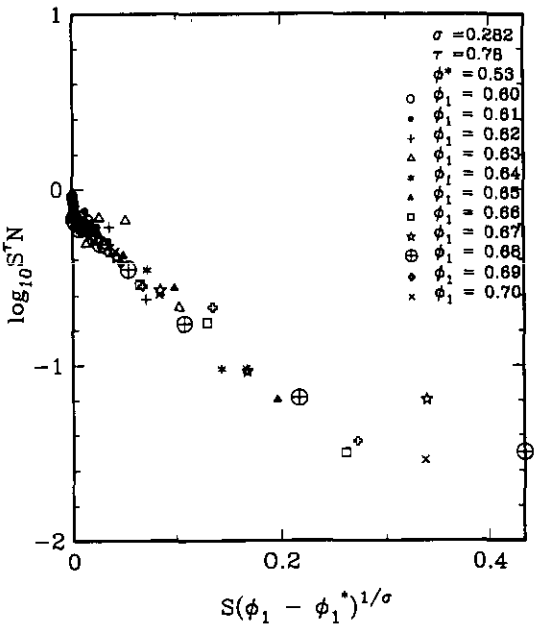

Figure 7. Scaling plot of the fragment size in terms of cells $S(f, c)$. Here $\log_{10} S(f, c)^{\tau(f,c)} N_{S(f,c)}$ is plotted as a function of $[\phi_1 - \phi_1^*(f, c)]^{1/\sigma(f,c)} S(f, c)$ as in relation (5). The best collapse of the data is for $\sigma(f, c) = 0.28$, $\tau(f, c) = 0.78$ and $\phi_1^*(f, c) = 0.53$.

and fragments in terms of cells. Comparing the values of scaling variables for bursts and groups as expressed in cells shows quantitatively the close relation between the two objects. It was initially expected that groups and fragments would exhibit such a close scaling relationship, due to the fact that these two objects as measured in cells are almost identical in size; in addition, the size of groups in terms of fragments is very close to 1. However, the data for bursts and groups indicate a much closer relationship than do fragments and bursts, at least in terms of the scaling behaviour.

In figure 8, scaling results for bursts as measured in number of fragments per burst are presented. Clearly the collapse of the data is not nearly as good as that seen in the previous figures for objects as measured in terms of cells. Here the best collapse was found to occur for $\tau(b, f) = 1.58$, $\sigma(b, f) = 0.21$ and $\phi_1^*(b, f) = 0.58$. The data for bursts in terms of groups showed even poorer collapse than did bursts as expressed in fragments. This case resulted in a critical mass fraction $\phi_1^*(b, g) = 0.41$, a value which seemed excessively low when compared with the previous results. This is a further indication that bursts and groups are too closely related for good scaling behaviour to be seen. The data for groups in terms of fragments were so closely distributed that no scaling was possible; note that the mean group size as measured in number of fragments was only slightly higher than 1 for all mass fractions examined.

An interesting result is that the optimum scaling for the three objects in terms of cells obeys relation (3) for the critical mass fractions $\phi_1^*(x, y)$. However, the estimated critical mass fraction for bursts in terms of fragments $\phi_1^*(b, f)$ does not obey the leftmost inequality of relation (4). Due to the relatively small number of bursts generated, it is not clear whether this is due to inaccuracies arising from a lack of data points or is an actual characteristic of the problem itself. However, since the computed value of $\phi_1^*(b, f) = 0.58$ lies very near the value found for $\phi_1^*(b, c) = 0.57$, it is clearly

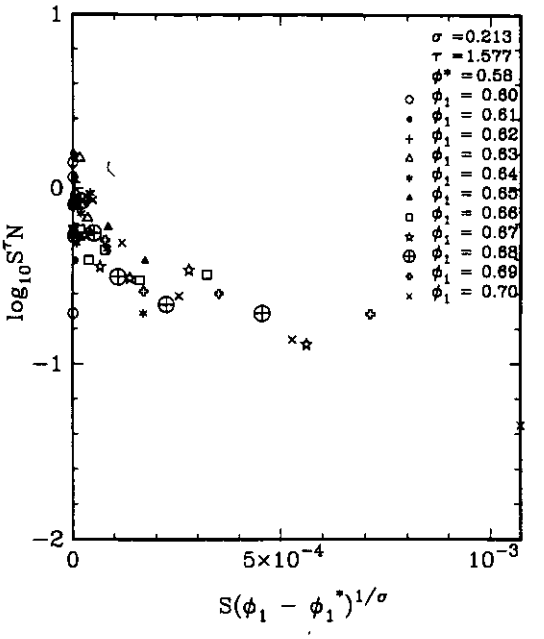

Figure 8. Scaling plot of the burst size in terms of fragments $S(b,f)$. Here $\log_{10} S(b,f)^{\tau(b,f)} N_{S(b,f)}$ is plotted as a function of $[\phi_1 - \phi_1^*(b,f)]^{1/\sigma(b,f)} S(b,f)$ as in relation (5). The best collapse of the data is for $\sigma(b,f) = 0.21$, $\tau(f,c) = 1.58$ and $\phi_1^*(f,c) = 0.58$.

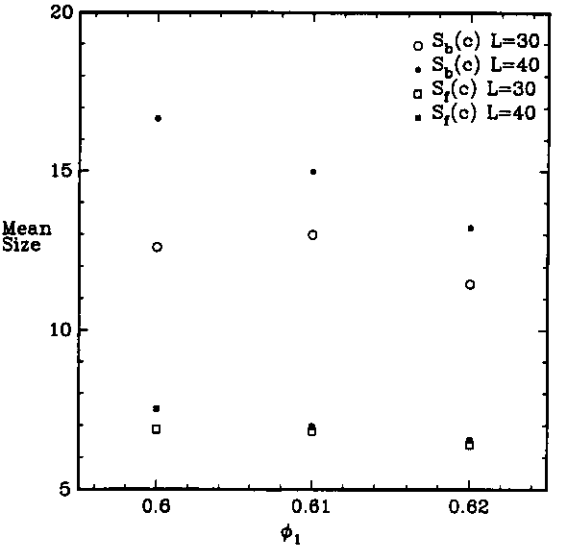

Figure 9. Effects of changing system size on the mean fragmentation object sizes. Open squares and circles denote data obtained at a system size of $L = 30$ for the mean burst size $S(b,c)$ and mean fragment size $S(f,c)$ in terms of cells, respectively. Filled squares and circles denote data obtained at a system size of $L = 40$ for the mean burst size $S(b,c)$ and mean fragment size $S(f,c)$ in terms of cells, respectively.

possible that further generation of data may result in an ordering of critical mass fractions as indicated in relation (4).

Not surprisingly, the best collapse of the data as measured by the sum of the squares of the errors was found for bursts in terms of cells $S(b, c)$. This result was expected, since $S(b, c)$ is a measure of the highest level objects (bursts) in terms of the lowest level sub-objects (cells), providing the largest range of sizes and exhibiting a relatively smooth distribution. As one measures objects in terms of sub-objects which are very closely related, such as groups in terms of fragments, the scaling breaks down. However, results for bursts, groups and fragments in terms of cells all showed relatively good scaling behaviour, most clearly in the smaller size ranges. The collapse of the data was not as good for the larger object sizes, reflecting the greater amount of scatter in these data.

As in any simulation of an infinite system, the finite size of the model system affects the results. As noted above, the model system used here was 30 cell lengths wide, with periodic boundaries in both x-directions. To determine the effects of this finite-sized system, additional runs of 3000 total bursts were made at the lowest reactive phase mass fractions ($\phi_1 = 0.60$, 0.61 and 0.62) with a system size of 40 cell lengths. In figure 9 we present the mean size of several fragmentation objects for the two system sizes studied. The mean sizes of all objects showed an increase with increasing system size, with the largest increases at the lower reactive phase mass fractions. At the lower values of ϕ_1, the data obtained at $L = 30$ began to decrease, rather than increase as would be expected. This trend was not observed for the larger system size, indicating that this decrease was due to finite system size effects rather than a characteristic of the fragmentation process itself.

5. Conclusions

One aspect of the complex process of fragmentation, namely the hindering of fragments from release, has been studied by using a two-dimensional model of a two-phase solid which undergoes a reaction at its surface. By employing scaling concepts of cluster percolation theory, new and interesting results describing the behaviour of the hindered fragmentation process have been obtained. The characterization of fragmentation in terms of a hierarchy of objects and their constituent sub-objects has revealed the subtle and unique percolation behaviour of the fragmentation process. In particular, the indication of different critical reactive mass fractions for different objects as defined by their respective sub-objects is unique to the hindered fragmentation process. A further interesting result is the indicated existence of 'virtual' critical mass fractions, i.e. critical points which cannot be reached due to the physical limitations of the problem, but which arise as properties of the scaling function. Although the intent of this study was to provide an introduction to the unique aspects of the hindered fragmentation problem, estimates of the scaling exponents and the critical mass fractions for various fragmentation quantities have been computed. In particular, the reported critical mass fractions for the highest level object (bursts) follow a postulated trend based on physical reasoning. The reported results have shown that hindered fragmentation can be described using percolation scaling concepts, allowing the characterization of fragmentation objects in terms of several different sub-objects, yielding readily interpreted dependencies of average properties on the reactive phase mass fraction.

Acknowledgments

C A Miller and S Torquato gratefully acknowledge the partial support of the Office of Basic Energy Sciences, US Department of Energy, under grant no DEFG05-86ER13482. Support for A R Kerstein was provided by the Division of Engineering and Geosciences, Office of Basic Energy Sciences, US Department of Energy.

References

Chirone R, Cammarota A, D'Amore M and Massimilla L 1982 *Nineteenth Intl. Symp. on Combustion* (Pittsburgh: Combustion Institute) p 1213

DeAngelis A R and Mekjian A Z 1989 *Phys. Rev.* C **40** 105

Deutscher G, Zallen R and Adler J (ed) 1983 *Percolation Structures and Processes* (*Annals of the Israel Physical Society* **5**) (Bristol: Adam Hilger)

Essam J W 1980 *Rep. Prog. Phys.* **43** 883

Kerstein A R and Niksa S 1983 *Intl. Conf. on Coal Science* (Pittsburgh: International Energy Agency) p 743

—— 1985 *Twentieth Intl. Symp. on Combustion* (Pittsburgh: Combustion Institute) p 941

Kerstein A R and Edwards B F 1987 *Chem. Eng. Sci.* **42** 1629

Kinzel W 1983 *Percolation Structures and Processes* vol 5, ed G Deutscher, R Zallen and J Adler (Bristol: Adam Hilger) p 425

Mekjian A Z 1990 *Phys. Rev. Lett.* **64** 2125

Mills B E and Kerstein A R 1990 unpublished

Nickel B and Wilkinson D 1983 *Phys. Rev. Lett.* **51** 71

Sevick E M, Monson P E and Ottino J M 1988 *J. Chem. Phys.* **88** 1198

Stauffer D 1979 *Phys. Rep.* **54** 1

—— 1985 *Introduction to Percolation Theory* (London: Taylor and Francis)

Sundback C A, Beér J M and Sarofim A F 1985 *Twentieth Intl. Symp. on Combustion* (Pittsburgh: Combustion Institute) p 1495

Wilkinson D and Willemsen J F 1983 *J. Phys. A: Math. Gen.* **16** 3365

Willemsen J F 1984 *Phys. Rev. Lett.* **52** 2197

Williams J K and Mackenzie N D 1984 *J. Phys. A: Math. Gen.* **17** 3343